High-Concentration Freeform Microtracking Concentrators With Single-Axis External Tracking

Håkon J. D. Johnsen[a)] and Jan Torgersen

Norwegian University of Science and Technology, Department of Mechanical and Industrial Engineering, Richard Birkelands Vei 2b, Trondheim, Norway

[a)]*Corresponding author: hakon.j.d.johnsen@ntnu.no*

Abstract. Microtracking concentrators enable the use of concentrator photovoltaics without the need for accurate two-axis external solar tracking. However, the wide tracking range required from stationary microtracking concentrators leads to designs with reduced concentration or complex designs with multiple moving surfaces. Additionally, stationary microtracking concentrators suffer from high cosine projection losses. We propose combining microtracking concentrators with low-precision horizontal single-axis trackers commonly used for conventional silicon photovoltaics. This reduces the demands of the microtracking concentrator while simultaneously reducing the cosine projection losses. We show how the performance in such a configuration can be boosted using a combination of freeform surfaces and a modified lenslet packing scheme and present a concentrator achieving 85% average yearly efficiency at a geometric concentration of 776x.

INTRODUCTION

Concentrator photovoltaics (CPV) enables highly efficient conversion of sunlight to electricity but requires highly accurate two-axis solar tracking. Microtracking solar concentrators use small-scale movements in the CPV module to perform this tracking inside the module, eliminating the need for external two-axis trackers [1]. Such microtracking can enable the use of high-efficiency CPV modules in space-constrained locations unsuitable for large-scale two-axis solar trackers and can help eliminate the costs associated with mechanically complex external trackers subject to substantial wind loads.

Microtracking concentrators need to have good optical performance across a large tracking range to be effective, making the optical design a challenging trade-off between optical efficiency, tracking range, and complexity. Previous research has demonstrated how it is possible to create high-performance complex designs with multiple moving surfaces [2, 3]. Less complex designs can be made from a single lens array at the cost of lower concentration [4, 5].

Microtracking with Horizontal Single-Axis Tracking

One option to reduce the tracking demands of microtracking concentrators is to combine them with a single-axis external solar tracker, which has the added benefit of reducing the cosine projection losses [3]. Using horizontal single-axis trackers might be especially interesting, as this configuration has been installed in large volumes for conventional unconcentrated photovoltaics and has been cited as a contributor to the reduction in costs of those systems [6].

Fig. 1a schematically shows a microtracking concentrator placed on a horizontal single-axis tracker. If we assume a specific installation location and orientation, the yearly angular distribution of insolation received by the concentrator can be simulated, as shown in Fig. 1b for an installation latitude of $40°$ north. The simulation is done using a simple geometrical model with air-mass attenuation and can easily be refined using real-world irradiance data from a target installation location.

As shown from Fig. 1, the required tracking range under horizontal single-axis tracking is still relatively wide, spanning approximately $30°$ to the north and $60°$ to the south at an installation latitude of $40°$. However, this tracking range is only needed about one axis. About the other axis, it is sufficient with a few degrees of tracking to compensate for tracking errors in the low-accuracy external tracker. Therefore, it might be possible to take advantage of this asymmetry by designing a microtracking concentrator with a broader tracking range about one axis and a reduced tracking range about the other axis. This can be achieved by using optics that are not rotationally symmetric, by stretching the aperture of the lenslets on the bottom surface, and by allowing for a cell that is rectangular instead of square.
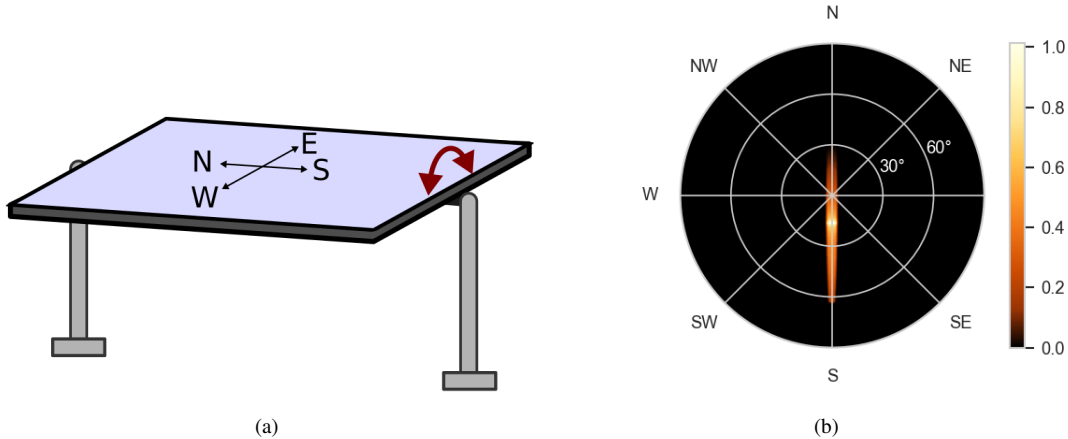
FIGURE 1. (a) A microtracking concentrator mounted on a north-south aligned horizontal single-axis external tracker. (b) Simulated normalized angular distribution of the insolation, as seen from the local coordinate system of the microtracking concentrator.

OPTIMIZATION APPROACH

Microtracking concentrators are commonly designed by selecting a specific tracking range and designing the module for good performance within this tracking range [3, 7]. However, choosing this tracking range becomes a choice between a short tracking range to allow for good optical performance when the sun is near-normal to the module, or a large tracking range to collect sunlight through as large a fraction of the day and year as possible.

To avoid choosing an explicit tracking range, we have adopted an optimization approach inspired by Ito et al. [4]. By selecting a target installation location and orientation, it becomes possible to define an average yearly efficiency as the weighted mean of optical efficiency across all angles of incidence, weighted by the fraction of insolation received at each angle. This average yearly efficiency thus shows what fraction of all sunlight received by the microtracking module across a year is successfully concentrated to the receiver surface.

We then use numerical optimization to design microtracking concentrators with as large a geometric concentration ratio as possible, using the average yearly efficiency as an optimization constraint. The resulting objective function is shown in Eq. 1.

$$\max f\left(\mathbf{x}, C_g\right) = C_g \tag{1}$$
$$\text{such that } \overline{\eta}\left(\mathbf{x}, C_g\right) \geq \eta_{target}, \tag{2}$$

where $\mathbf{x}$ is a parametrization of the concentrator geometry, C_g is the geometric concentration ratio, $\overline{\eta}\left(\mathbf{x}, C_g\right)$ is the average yearly efficiency of the concentrator and η_{target} is the target average yearly efficiency.

This objective function causes the optimization algorithm to search for the concentrator that can successfully concentrate a fraction η_{target} of all sunlight received over the year, using a geometric concentration ratio that is as large as possible.

We optimize the concentrators using a memetic optimization algorithm constructed by combining the Differential Evolution and the SLSQP algorithms from Scipy [8]. The optimization was done on computing resources provided by the NTNU IDUN/EPIC computing cluster [9].

DESIGN EXAMPLES

Using the presented objective function and optimization approach, we optimized two different design examples for an 85% average yearly efficiency when placed on a horizontal single-axis external tracker at a latitude of 40°.

The first design example was made using conventional assumptions of rotationally symmetric optical surfaces, using hexagonally packed lenslets and square cells. The second design example was made using freeform surfaces

TABLE I. Optimization parameters of the two design examples. Design 1 is designed using conventional rotationally symmetric surfaces, while design 2 is design with freeform surfaces.

Parameter	Design 1	Design 2
Surface type	Asphere	Freeform
Surface representation	QCon Polynomial	Even-ordered Legendre polynomial
Lens aperture	Hexagonal	Hexagonal + Stretched polygon
Receiver shape	Square	Rectangular
Target average yearly efficiency	85%	85%
Resulting concentration (optimiztion results)	$C_g = 218$	$C_g = 776$

TABLE II. Simulation parameters used when optimizing both of the design examples

Parameter	Value
Latitude	$40°$
External solar tracking	Horizontal single-axis tracking
External tracking accuracy	$\pm 3°$
Sunshape	Top-hat with $0.27°$ half-angle
Solar spectrum	AM1.5D
Reflection losses	Yes
Absorption losses	No[a]
Material	PMMA
Average yearly efficiency	85%

[a] In this preliminary optimization, all dimensions are relative and not fixed to a specific size. Volumetric absorption losses are therefore not well-defined.

and a stretched aperture on the rear surface designed to be more conducive to a wide tracking range in one direction. This way, we could explore what kind of performance can be achievable under horizontal single-axis tracking, and how much of this can be ascribed to breaking the rotational symmetry of the optics.

The surfaces of the rotationally symmetric design were aspheres represented using a Forbes QCon Polynomial [10].

The surfaces of the second, freeform, design were represented using even-ordered Legendre polynomials. By only using even-ordered terms, the resulting freeform surface remains symmetric about the x and y axes and was done for simplicity. Including the odd terms in the north-south direction might further improve the performance but was not done at this initial stage because it is easier to work with systems that still have some symmetry. The lens surfaces on the rear side of the lens array had a stretched aperture, as shown in Fig. 2. A comparison between the optimization parameters of the two designs is shown in Table I.

The systems were simulated using a custom ray-tracer implemented in Python and compiled to native code using Numba [11]. Parameters used for the simulations of both designs are shown in Table II.
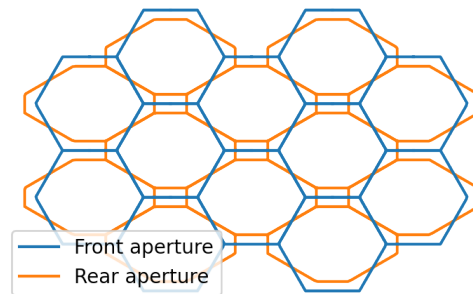

FIGURE 2. Illustration of how the aperture of the rear lenslets in Design 2 have been elongated in one direction to increase tracking range about one axis, while still being aligned to the hexagonal packing of the front apertures.

RESULTS

Figure 3 shows the two optimized design examples. The rotationally symmetric Design 1 achieved a geometric concentration ratio of $C_g = 218$, while Design 2 achieved a geometric concentration ratio of $C_g = 776$. This demonstrates that significant concentration gains can be achieved for microtracking concentrators placed on horizontal single-axis trackers, given that we use a microtracking configuration that can take advantage of the strong asymmetry in the required tracking range.
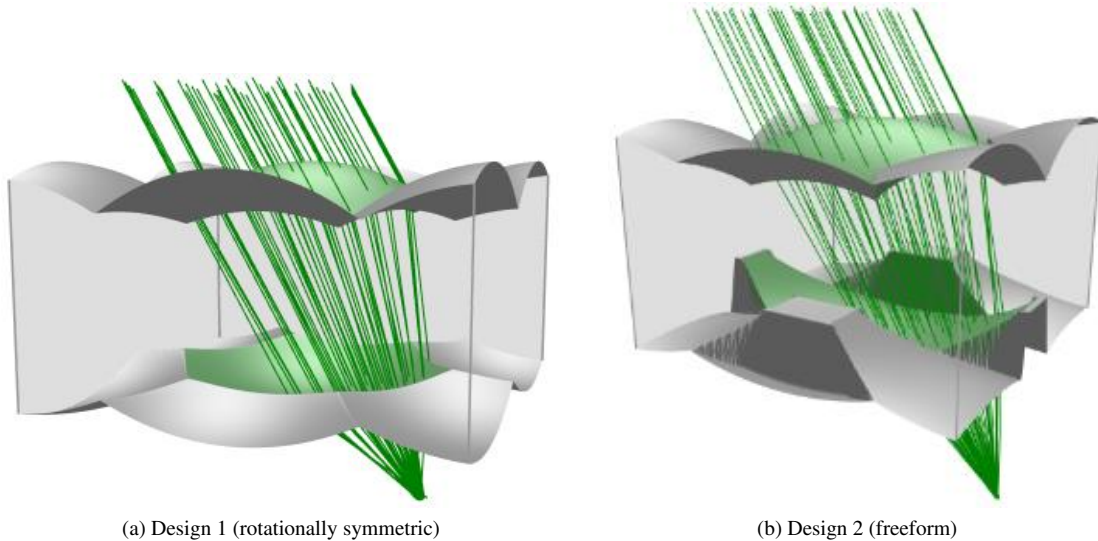

(a) Design 1 (rotationally symmetric)   (b) Design 2 (freeform)

FIGURE 3. 3D-model of the two design examples, with rays traced through one of the lenslets (highlighted in green). Both designs are shown at a $30°$ angle of incidence.

Figure 4 further shows the distinction between Design 1 and 2 by comparing their tracking ranges. Design 1 efficiently tracks in the range of angles required (those from Fig. 1b), but due to the inherent rotational symmetry of the optics, the design also tracks effectively in an extensive range of angles where it is not needed. (The performance in Fig. 4a is still not fully rotationally symmetric due to the hexagonal outline of the lenses and the square outline of the simulated cell.) Design 2, on the other hand, is no longer rotationally symmetric, and the optimization algorithm has not prioritized efficiency for wide angles in the east-west direction where a large tracking range is not needed.
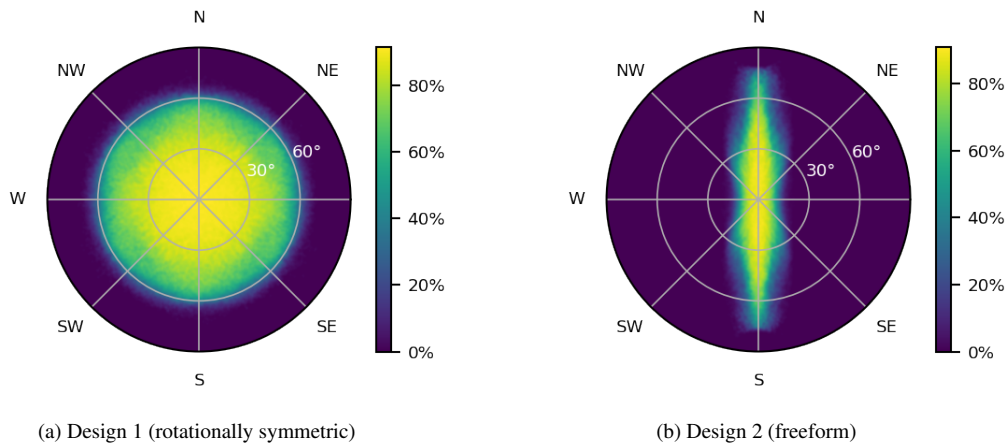

(a) Design 1 (rotationally symmetric)   (b) Design 2 (freeform)

FIGURE 4. Efficiency of the two example designs at different angles of incidence. Both designs have been optimized to achieve an average yearly efficiency of 85% under the yearly angular distribution of sunlight shown in Fig. 1b.

The irradiance distribution on the simulated cells is shown in Fig. 5 for some different incidence angles. For each angle of incidence, rays are traced from the $\pm 0.27°$ top-hat angular distribution and the AM1.5D spectrum. The figure shows how both Design 1 and Design 2 have a sharp focal spot at $0°$ angle of incidence, but Design 1 cannot maintain this focal spot at larger angles of incidence, making it necessary to use a larger simulated cell geometry. Design 2, on the other hand, has been able to accurately control the shape of the focal spot across the whole tracking range, enabling the factor of 3.5 increase in geometric concentration factor compared to the rotationally symmetric case.
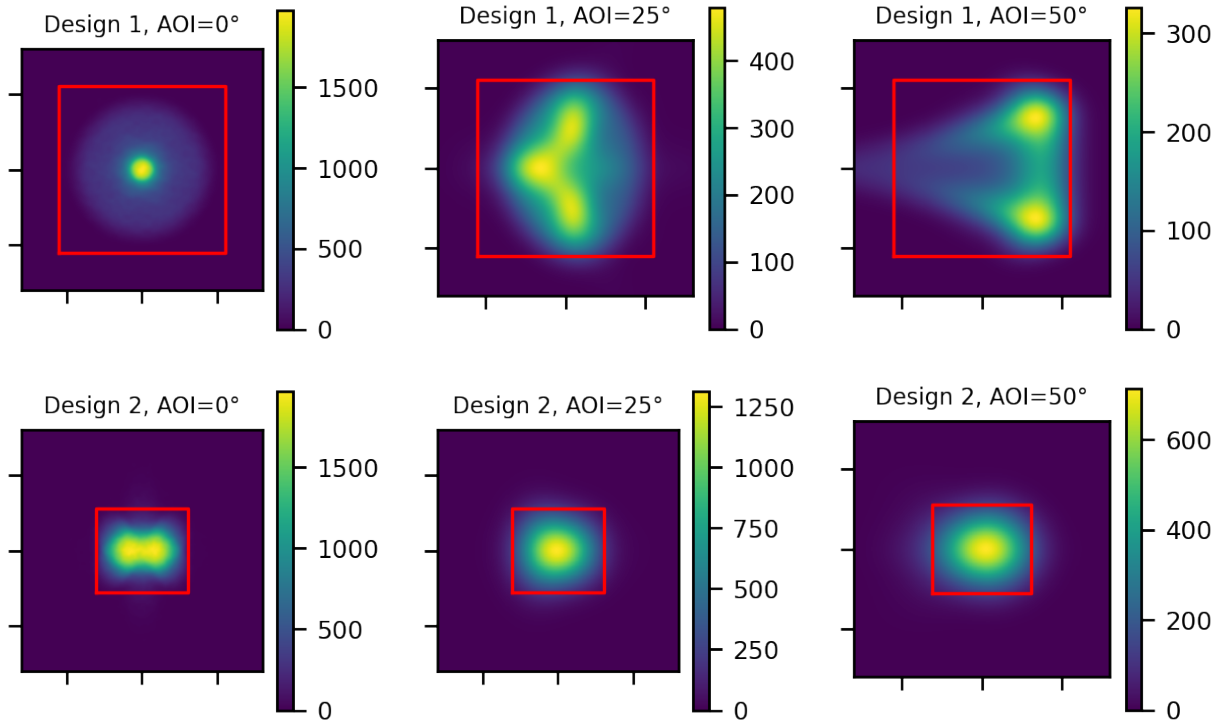

FIGURE 5. Simulated irradiance distribution from the two design examples, at different angles of incidence. The red square/rectangle represents the simulated cell area, and the colorbars represent irradiance normalized to 1 sun. All axes have the same dimensions (but values are not shown because absolute system dimensions have not been specified in this preliminary optimization and all dimensions are relative).

DISCUSSION AND CONCLUSION

The presented results show that the concentration ratio of microtracking concentrators under one-axis external tracking can be significantly improved using freeform optics without increasing the number of optical surfaces. This is possible because the additional degrees of freedom allow the designs to be directly tailored to the asymmetric tracking requirements (as given by Table II). The rotationally symmetric design, on the other hand, is optimized under the same conditions but is not able to take advantage of these asymmetries.

The design examples are made using the very optimistic assumptions of ideal surface geometry and $\pm 0.27°$ top-hat angular distribution of sunlight. Therefore, the reported geometric concentration ratios are expected to have to be lowered in real-world implementations of the concentrators to account for non-ideal manufacturing tolerances, nonzero circumsolar radiation, and non-zero tracking errors. Further work may involve repeating the presented optimization with a model that considers such effects.

There are still several additional degrees of freedom available in the design of a freeform concentrator not considered in this paper. This includes using the odd terms of the Legendre polynomial, using an offset between the front- and the back apertures, and squeezing the front apertures in the x- or y-direction. Further work may therefore take

such extra degrees of freedom into account to potentially gain even better control over the focal spot over a large field of view.

In summary, we have shown that microtracking concentrators can be combined with horizontal single-axis trackers to reduce the demands on the microtracking and offset some of the cosine losses of stationary microtracking concentrators. Furthermore, we showed how it is necessary to break the rotational symmetry of the concentrator to take full advantage of the reduced tracking requirements and that a freeform concentrator in the proposed configuration can achieve a geometric concentration of 776x at 85% average yearly efficiency. While still preliminary, these results indicate one potential path towards increasing the performance of microtracking concentrators while taking advantage of developments and equipment from conventional unconcentrated photovoltaics.

REFERENCES

1. H. Apostoleris, M. Stefancich, and M. Chiesa, "Tracking-integrated systems for concentrating photovoltaics," Nature Energy **1**, 16018 (2016).
2. H. J. D. Johnsen, J. Torgersen, and A. Aksnes, "High-concentration wide-angle tracking integration with stacked lens arrays," AIP Conference Proceedings **2149**, 070005 (2019).
3. F. Duerr, Y. Meuret, and H. Thienpont, "Tailored free-form optics with movement to integrate tracking in concentrating photovoltaics," Optics Express **21**, A401–A411 (2013).
4. A. Ito, D. Sato, and N. Yamada, "Optical design and demonstration of microtracking CPV module with bi-convex aspheric lens array," Optics Express **26**, A879–A891 (2018).
5. G. Nardin, C. Domínguez, Á. F. Aguilar, L. Anglade, M. Duchemin, D. Schuppisser, F. Gerlich, M. Ackermann, L. Coulot, B. Cuénod, D. Petri, X. Niquille, N. Badel, A. Lachowicz, M. Despeisse, J. Levrat, C. Ballif, S. Askins, R. Núñez, N. Jost, G. Vallerotto, and I. Antón, "Industrialization of hybrid Si/III–V and translucent planar micro-tracking modules," Progress in Photovoltaics: Research and Applications **29**, 819–834 (2021).
6. H. Apostoleris, S. Sgouridis, M. Stefancich, and M. Chiesa, "Evaluating the factors that led to low-priced solar electricity projects in the Middle East," Nature Energy , 1 (2018).
7. J. S. Price, X. Sheng, B. M. Meulblok, J. A. Rogers, and N. C. Giebink, "Wide-angle planar microtracking for quasi-static microcell concentrating photovoltaics," Nature Communications **6**, 6223 (2015).
8. P. Virtanen, R. Gommers, T. E. Oliphant, M. Haberland, T. Reddy, D. Cournapeau, E. Burovski, P. Peterson, W. Weckesser, J. Bright, S. J. van der Walt, M. Brett, J. Wilson, K. J. Millman, N. Mayorov, A. R. J. Nelson, E. Jones, R. Kern, E. Larson, C. J. Carey, İ. Polat, Y. Feng, E. W. Moore, J. VanderPlas, D. Laxalde, J. Perktold, R. Cimrman, I. Henriksen, E. A. Quintero, C. R. Harris, A. M. Archibald, A. H. Ribeiro, F. Pedregosa, P. van Mulbregt, and Scipy 1.0 Contributors, "SciPy 1.0: Fundamental algorithms for scientific computing in Python," Nature Methods **17**, 261–272 (2020).
9. M. Själander, M. Jahre, G. Tufte, and N. Reissmann, "EPIC: An Energy-Efficient, High-Performance GPGPU Computing Research Infrastructure," arXiv:1912.05848 [cs] (2021), arXiv:1912.05848 [cs].
10. G. W. Forbes, "Shape specification for axially symmetric optical surfaces," Optics express **15**, 5218–5226 (2007).
11. S. K. Lam, A. Pitrou, and S. Seibert, "Numba: A LLVM-based Python JIT Compiler," in *Proceedings of the Second Workshop on the LLVM Compiler Infrastructure in HPC*, LLVM '15 (ACM, New York, NY, USA, 2015) pp. 7:1–7:6.